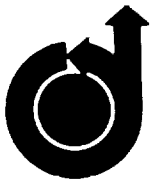

AIAA 80-1556R
Pressures Around an Inclined Ogive Cylinder with Laminar, Transitional, or Turbulent Separation

P. J. Lamont

Reprinted from
AIAA Journal Volume 20, Number 11, November 1982, Page 1492

AMERICAN INSTITUTE OF AERONAUTICS AND ASTRONAUTICS • 1290 AVENUE OF THE AMERICAS • NEW YORK, NEW YORK, N.Y. 10104

AIAA 80-1556R

Pressures Around an Inclined Ogive Cylinder with Laminar, Transitional, or Turbulent Separation

P.J. Lamont*
NASA Ames Research Center, Moffett Field, California

This paper reports results from comprehensive pressure tests on an ogive cylinder in the low-turbulence 12-ft pressure wind tunnel at Ames Research Center. The results consist of detailed pressure distributions over a wide range of Reynolds numbers (0.2×10^6 to 4.0×10^6) and angles of attack (20 to 90 deg). Most important, the tests encompassed a complete coverage of different roll orientations. This variation of roll orientation is shown to be essential in order to fully define all the possible flow conditions. When the various roll-angle results are combined, it is possible to interpret correctly the effects of changing angle of attack or Reynolds number. Two basic mechanisms for producing asymmetric flow are identified. One mechanism operates in both the laminar and the fully turbulent separation regimes; this mechanism is the one qualitatively described by the impulsive flow analogy. The other mechanism occurs only in the transitional separation regime. This asymmetric flow has the same form as that found in the two-dimensional cross flow on a circular cylinder in the transitional flow regime. Finally, these results make it possible to draw up critical Reynolds number boundaries between the laminar, transitional, and fully turbulent separation regimes throughout the angle-of-attack range from 20 to 90 deg.

Nomenclature

CND	= local normal-force coefficient, local normal force/$(qD\sin^2\alpha)$
CNO	= overal normal-force coefficient, overall normal force/$(q\pi D^2/4)$
C_p	= cross flow pressure coefficient, $(p-p_\infty)/(q\sin^2\alpha)$
CYD	= local side-force coefficient, local side force/$(qD\sin^2\alpha)$
CYO	= overall side-force coefficient, overall side force/$(q\pi D^2/4)$
CYO_{max}	= maximum overall side force recorded in a roll sweep
D	= cylinder diameter
L	= length of instrumented section (6 diameters)
p	= pressure on model surface
p_∞	= freestream static pressure
q	= freestream dynamic pressure
R	= cylinder radius, $D/2$
Re_D	= Reynolds number, UD/ν
U	= freestream velocity
x	= axial distance from nose tip
α	= angle of attack
θ	= azimuth angle around circular cross section measured from windward generator
ν	= kinematic viscosity
ϕ	= roll angle
$\|\ \|$	= modulus of included parameter

Introduction

THE flow over slender bodies of revolution at high angles of attack has been studied extensively, both experimentally and mathematically, in the last ten years. Interest in this subject is partly a practical response to the needs of aircraft and missile designers who wish to improve maneuverability by extending flight envelopes to higher angles of attack. However, a great deal of the interest is a result of the intrinsic fascination of a flow in which an axisymmetric body can produce an asymmetric flow pattern and, hence, experience a side force.

The fascination of the subject seems to have been matched by the difficulties it has posed to both experimentalists and computationalists. The computational difficulties are not surprising since the flow is an extremely complex three-dimensional one involving separation lines that are not fixed at sharp edges and a large turbulent wake. Much fundamental work and further advances in computer hardware will be required before such flows can be computed. It is the difficulties met by experimentalists that are, at first sight, so surprising.

It would seem to be a simple matter to test an ogive-cylinder body throughout the angle-of-attack range from 0 to 90 deg at a particular Reynolds number and Mach number and to produce variations of normal force and side force with angle of attack that would be universally valid for the stated test conditions. Similarly, it would seem to be easy to vary body geometry, Reynolds number, and Mach number and to find their effect on the forces on the body. On the contrary, a study of the extensive published work on this topic shows that it has not been easy to do these things. Certain trends do emerge from the literature, but there are numerous discrepancies and inconsistencies between the results of different workers.

The testing problems that are mentioned in the literature include flow unsteadiness, model unsteadiness, and variations with model roll angle. In addition, difficulties have arisen in interpreting the effect of Reynolds number. In two-dimensional cylinder flow it has been common practice to quote "critical" Reynolds numbers that mark the boundaries between different flow conditions. These flow conditions are determined principally by the state of the boundary layer at separation. These different flow conditions are loosely referred to as laminar, transitional, or turbulent. Similar classifications and critical Reynolds numbers have been sought for bodies of revolution at angle of attack. The

Received Aug. 9, 1980; presented as Paper 80-1556 at the AIAA 7th Atmospheric Flight Mechanics Conference, Danvers, Mass., Aug. 11-13, 1980; revision received March 15, 1982. This paper is declared a work of the U.S. Government and therefore is in the public domain.

*NRC Research Associate; presently, Lecturer, Department of the Mechanics of Fluids, University of Manchester, England. Member AIAA.

problems have arisen in determining the correct variation of these critical Reynolds numbers with angle of attack.

This paper presents results from a wind-tunnel test program that was designed to overcome most of the experimental difficulties just mentioned. The program was an attempt to investigate fully the effect of Reynolds number and roll angle at low subsonic Mach numbers for one particular configuration, an ogive cylinder with a 2-diameter tangent ogive nose.

Experimental Details

This section considers the experimental difficulties in more detail and describes how they were overcome in this particular test program. It also gives details of the model, its instrumentation, and the range of variation of the test parameters.

The problem of flow unsteadiness was minimized by selecting a wind tunnel for the testing that had a very low turbulence level. This follows the hypothesis put forward in a previous paper by Lamont and Hunt[1] that suggests that much of the flow unsteadiness is caused by turbulence in the freestream. Thus, flow unsteadiness would be reduced in conditions of very low freestream turbulence. The wisdom of this approach has already been confirmed by the recent results of Hunt and Dexter.[2] The wind tunnel chosen for the present tests was the 12-ft pressure wind tunnel at Ames Research Center; the tunnel has a freestream turbulence level of about 0.05% and the additional advantage of being able to reach a Reynolds number of 26×10^6/m (8×10^6/ft).

Fig. 1 Model installed in wind tunnel.

The model instrumentation was chosen carefully to minimize experimental problems and maximize the information provided about this complex flow. Surface pressure measurements were taken in preference to using a force balance; this was done for the following reasons. The surface pressures can be integrated to give the same overall normal and side forces and moments that might be recorded by a force balance. However, the pressure-tapped model can be mounted much more rigidly than would be possible with a strain gage balance system. Hence, model motion was eliminated as a source of flow unsteadiness and possible flow modification. In addition to overall forces and moments, the pressure measurements provide details of normal- and side-force distributions along the body which are extremely useful in the analysis of this complex three-dimensional flow. Finally, the pressure distributions at different cross sections along the body can be inspected and the state of the boundary layer can be deduced from their form, given a knowledge of two-dimensional cylinder flow.

The study of variations caused by changing the model's roll orientation was facilitated by including a remotely controlled roll mechanism in the model support. The model could be set at any roll angle between 0 and 350 deg from the chosen datum. Figure 1 shows the model and its support system installed in the wind tunnel. The model was made to very close tolerances and had a surface finish of nearly 0.13-μm (5-μin.) rms. It comprised a 2-diameter-long tangent ogive nose, a 6-diameter-long cylindrical forebody in front of the supporting pitch axis, and a 7-diameter-long cylindrical afterbody behind this axis. These cylindrical sections were 152.4 mm (6 in.) in diameter. The pressure instrumentation was confined to the first 6 diameters behind the nose tip and was thus well forward of the support axles. Inspection of the pressure distributions at the last station $x/D = 6$ yields no evidence of flow distortion or boundary layer transition caused by the presence of the support axles at $x/D = 8$. The 432 pressure tappings were arranged in rings of 36 (every 10 deg around the circumference of the model) at 12 stations along the model's axis. In addition to the just noted time-averaged pressure tappings, 48 miniature pressure transducers for measuring unsteady pressures were located in rings of 12 (every 30 deg around the circumference of the model) at 4 stations along the body to monitor fluctuating pressures. A sketch of the model, showing the positions of these pressure tappings, is shown in Fig. 2.

This ogive-cylinder model was tested throughout the angle-of-attack range from 20 to 90 deg. At least 12 roll orientations were tested at each angle of attack other than 90 deg. Results were obtained at eight Reynolds numbers (based on body

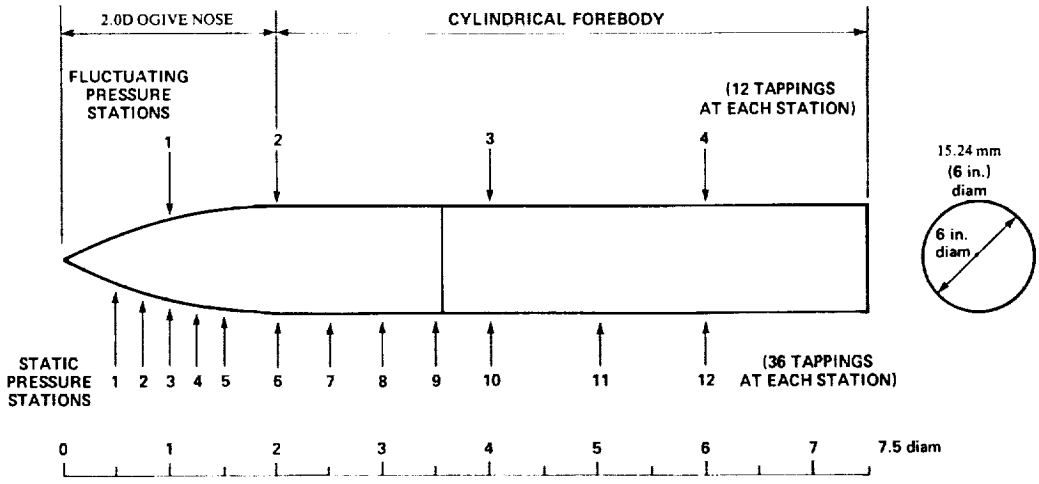

Fig. 2 Sketch of instrumented section of model showing positions of pressure-tapped stations.

diameter) between 0.2×10^6 and 4×10^6 and at Mach numbers of 0.3 or less. This represents the most comprehensive variation of angle of attack, roll angle, and Reynolds number ever attempted; the Reynolds number of 4×10^6 is the highest at which such tests have been conducted. This paper presents only a small fraction of the results obtained in this test program. All of the data will be made available in the near future in a NASA report.

Experimental Results

The output from the fluctuating pressure sensors mounted in the model was not only monitored during the tests but was also recorded on tape for future analysis. It was apparent immediately that the choice of a low-turbulence wind tunnel and the use of a carefully made, rigidly supported model had produced the hoped-for absence of serious flow unsteadiness. Therefore, the remainder of this paper presents only time-averaged pressure data. However, study of the results at different roll orientations revealed that variations with roll angle occur even though the flow is steady, and this variation with roll angle is a very significant feature of the results. The true effect of Reynolds number and angle of attack cannot be determined until the roll angle effect has been fully examined. Therefore, this section, which presents some of the experimental results, begins with a subsection on the roll-angle effect. This is followed by subsections devoted to side force and normal force throughout the Reynolds number and angle-of-attack range covered in this testing. The final subsection deals with the effect of angle of attack on the critical Reynolds numbers, which mark the boundaries between the laminar, transitional, and fully turbulent separation regimes.

Roll-Angle Effect

In general, 12 roll-angle settings were investigated at each angle of attack and Reynolds number. The pressure distributions obtained in these tests were integrated to find overall side forces and normal forces on the instrumented section of the ogive cylinder (i.e., the first 6 diameters). The overall side-force coefficient (CYO) varied between approximately equal positive and negative limits as roll angle ϕ was altered between 0 and 360 deg from the chosen datum. There were usually one to two cycles of this side-force variation within one revolution of the body. Generally, the 12 values of CYO were randomly distributed between the equal positive and negative limits. Only in a few cases did the plots of CYO vs ϕ tend toward a "square" waveform where most of the CYO results are of approximately equal value—half positive and half negative. In these cases, crossover between positive and negative values took place over about 20 to 30 deg of roll angle.

An example of the square waveform variation of side force with roll angle is shown in Fig. 3, together with the corresponding variation of normal force. These results are taken from tests with the ogive cylinder at 55 deg angle of attack and a Reynolds number (based on cylinder diameter) of 3×10^6. Run A represents results from a roll sweep, where data were obtained every 10 deg of roll. Solid symbols represent repeat tests at 140 and 300 deg roll. Run B represents results from a "standard" test where 12 roll angles (every 30 deg) were sampled at the same test conditions. The first thing to notice from this figure is the good repeatability of the results. Two "mirror image" states appear where the modulus of the overall side-force coefficient |CYO| is just less than 4. However, there are a number of in-between results, even in this example, which was chosen specially for its square waveform. These results include a result at 300 deg roll angle where the side force is nearly zero. Figure 3 also illustrates the large variation of the corresponding normal-force coefficient that occurs as the model is rolled.

Pressure measurements were chosen in preference to force-balance results because they provide additional useful information, including distributions of forces along the body. Figures 4 and 5 show how the distributions of side- and normal-force coefficients (based on cross flow dynamic pressure) vary at 12 different roll orientations for the same test conditions ($\alpha = 55$ deg, $Re_D = 3 \times 10^6$). Figure 4 shows that both the amplitude and the span of the side-force distribution vary at different roll orientations. High-peak local side force is accompanied by a shorter extent of the first half cycle; lower-peak local side force is accompanied by

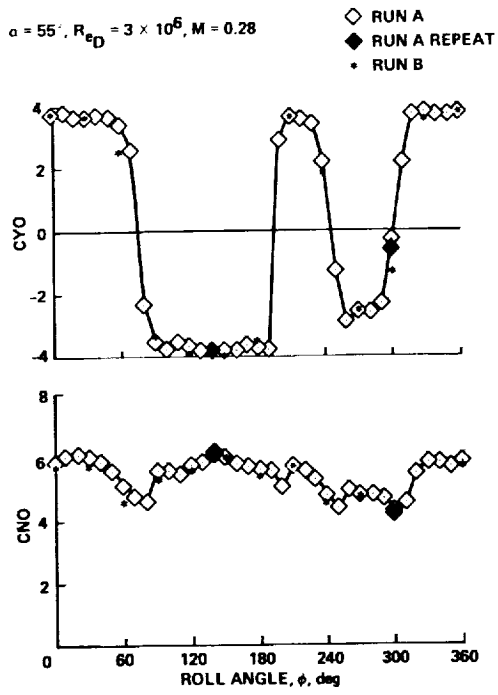

Fig. 3 Variation of overall force coefficients with roll angle.

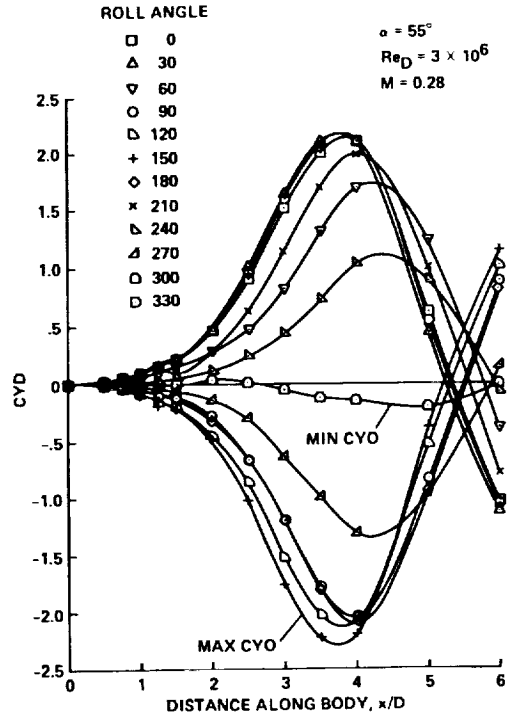

Fig. 4 Side force distributions along body at various roll angles.

progressively longer extent. Note that there is probably an upper limit to this increase in extent. The highest peak, shortest span distribution (the $\phi = 150$ deg result) produces the maximum value of overall side-force coefficient CYO. Note that the minimum overall side force (the $\phi = 300$ deg result) is produced by nearly symmetric flow over the whole length of the instrumented section and not by two equally balanced asymmetric flow regions. Figure 5 shows how varying roll orientation produces significant changes in the normal force distribution. Note that minimum overall normal force, as well as minimum overall side force, occurs at $\phi = 300$ deg and maximum overall normal force together with maximum overall side force occurs at $\phi = 150$ deg. Increased side force is accompanied by increased normal force for this case, which represents an example from the fully turbulent separation regime (see the later section on critical Reynolds numbers for details of how the flow was classified into different separation regimes).

When examining these data, one wonders why these dramatic changes are brought about by changing the roll orientation of a supposedly axisymmetric body. Support interference, if any occurs, is the same at each roll orientation. For these tests, flow unsteadiness is low and appears to be of the same order for both high and low side-force cases. Therefore, the changes must result from geometric variations departing from the ideal axisymmetric body which was specified. However, these variations are so slight over most of the model as to be almost undetectable. The only part of the model where there can be any significant variations from roundness is very near the nose tip. Perhaps asymmetries near the nose tip influence the flow over the whole model. A detailed study of the nose-tip geometry is planned for the second phase of this test program, in which an ogive cylinder with a 3.5-diameter-long ogive nose will be tested.

At present, the important details of the geometric asymmetries and their correlation with variations of the flow pattern are not known. However, the results from this test program were studied to see if there was any pattern to the variation of side force with roll angle that persisted despite changes in angle of attack and Reynolds number. Comparison of results is facilitated by nondimensionalizing the individual CYO results at a particular roll angle by the modulus of the maximum value of overall side-force coefficient $|CYO_{max}|$ recorded in its particular complete roll sweep. Hence, all these variations of $CYO/|CYO_{max}|$ will vary between limits of ± 1.0 for a complete revolution of the model. First, consider results in the fully turbulent separation regime. If all the results, at angles of attack where significant side forces occur (i.e., 40-70 deg) are plotted together, then results are confined to the band shown in Fig. 6. Although this band is quite wide at certain roll angles, it does suggest that there is some pattern to all the results in the fully turbulent separation regime. Although not plotted, the results at a Reynolds number of 0.2×10^6 (the only cases with fully laminar separation) also showed a pattern throughout the angle-of-attack range. In this case two roll angles (30 and 210 deg) gave high side forces; the rest gave near-zero values. These results are considered to be atypical of the laminar separation regime, possibly because a Reynolds number of 0.2×10^6 is too close to the boundary with the transitional flow regime. However, at other Reynolds numbers where transitional separation occurs no pattern persists for different angles of attack. One of the many examples that contrast with the pattern for fully turbulent separation cases is also plotted in Fig. 6.

It must be concluded that although there is some pattern to the variation with roll angle within the laminar and fully turbulent separation regimes, no such pattern exists for transitional separation cases. This highlights the need to test numerous roll orientations before any meaningful comparisons can be made between laminar, transitional, and turbulent flow.

The particular pattern of variation with roll angle found in these tests for fully turbulent separation cases can have no general significance, for it must be produced by the particular geometric asymmetries of this model. Another model made to the same specification would have different geometric asymmetries and, hence, produce a different roll-angle dependence. However, the square waveform of some of the results and the similarity of their positive and negative limits suggest that the maximum levels of side force may be applied generally between ogive cylinders of the same specified geometry. Indeed, recent results by Dexter and Hunt,[3] who tested two different $L/D = 3$ ogive noses on a cylindrical afterbody in the laminar separation regime and measured the same maximum side force, provide evidence for this belief.

Side Forces

The results presented in the previous subsection indicate that it is essential to test at a variety of roll orientations in order to define fully all the possible flow conditions. Only then is it possible to determine meaningful variations with angle of attack and Reynolds number that will have general significance for other ogive cylinders of the same nominal geometry. The most important side-force results are the maximum values recorded at a particular angle of attack and Reynolds number.

The variation of maximum overall side-force coefficient CYO_{max} with angle of attack is plotted in Fig. 7 for four of the eight Reynolds numbers that were tested. Results for

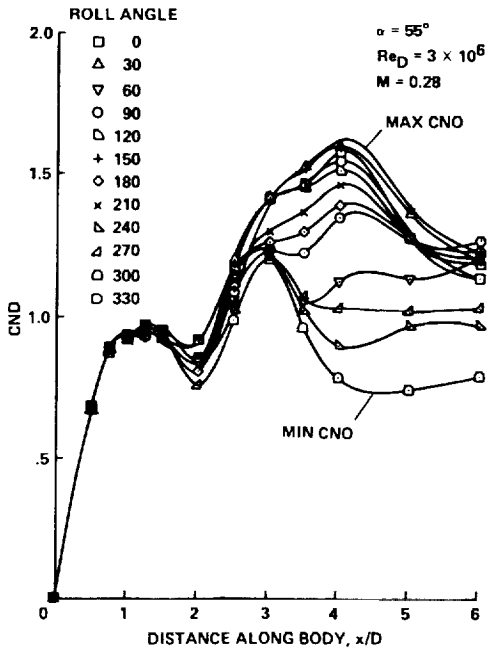

Fig. 5 Normal force distributions along body at various roll angles.

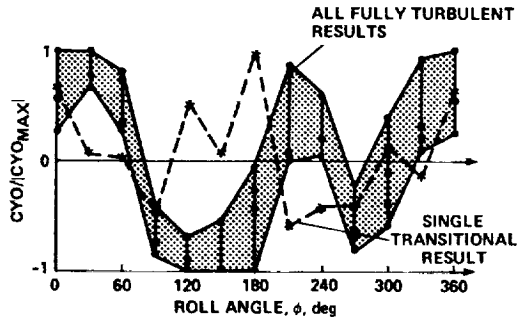

Fig. 6 Pattern of side force variation with roll angle.

Reynolds numbers of 0.2×10^6 and 4.0×10^6 represent laminar and fully turbulent separation cases, respectively, throughout the 20-90 deg angle-of-attack range. The results for Reynolds numbers of 0.4×10^6 and 0.8×10^6 correspond to transitional separation for most of this incidence range. The laminar and fully turbulent results are remarkably similar and show a greater side force than the transitional results for all angles of attack up to about 70 deg. Between angles of attack of 70 and 90 deg, transitional separation cases can produce larger side forces. The high maximum value at an angle of attack of 80 deg and a Reynolds number of 0.4×10^6 was only recorded at 2 of the 12 roll angles tested, whereas the high maximum value recorded at an angle of attack of 55 deg and a Reynolds number of 4.0×10^6 was approached at 9 of the 12 roll angles tested. One further comment about the transitional separation results at $\alpha=80$ deg and $Re_D=0.4\times10^6$; the side force at a roll orientation of 30 deg could be high or near zero, depending on the direction from which this roll angle was approached. This marked nonrepeatability only occurred for transitional separation cases.

The effect of Reynolds number on the maximum side force is illustrated by Fig. 8. The maximum side force (taken from a sample of at least 12 different roll angles) at an angle of attack of 55 deg is plotted in this figure at each of the test Reynolds numbers. The maximum side force falls from a high value at a Reynolds number of 0.2×10^6 (laminar separation) to almost zero in the middle of the transition region before climbing again to a higher level at Reynolds numbers of 2.0×10^6 to 4.0×10^6 (fully turbulent separation). This form of variation with Reynolds number is common to the angle-of-attack range from 45 to 70 deg. The Reynolds number range of 0.8×10^6 to 1.0×10^6, at which the near-zero side forces were recorded, is the same range of Reynolds number in which the minimum drag coefficient on a two-dimensional cylinder occurs and in which no coherent vortex shedding can be detected.

The axial distributions of side force that correspond to four of the points on Fig. 8 at Reynolds numbers of 0.2×10^6, 0.4×10^6, 0.8×10^6, and 4.0×10^6 are plotted together in Fig. 9. The similarity of maximum overall side forces at Reynolds numbers of 0.2×10^6 (laminar) and 4.0×10^6 (fully turbulent) is produced by very similar force distributions. The force distribution at a Reynolds number of 0.4×10^6 is completely different from those mentioned earlier, and that at a Reynolds number of 0.8×10^6 confirms the virtual disappearance of asymmetric flow at this Reynolds number.

Despite the similarity between both the overall side force and its distribution for laminar ($Re_D=0.2\times10^6$) and fully turbulent separation ($Re_D=4.0\times10^6$), the forces result from different pressure distributions around the body. Figure 10 presents pressure distributions, taken from tests at an angle of attack of 55 deg, to illustrate this point; the station chosen is $x/D=3$. Although the local side-force coefficients CYD are almost identical (equal enclosed areas of curves), their forms reflect the differing nature of the boundary layer at separation. The laminar case (solid line, $Re_D=0.2\times10^6$) shows poor pressure recovery after the first pressure minimum (around 60 deg) and early separation of the boundary layer at $|\theta|=80$ deg on one side and $|\theta|=90$ deg on the other. The fully turbulent case (dashed line, $Re_D=4.0\times10^6$) shows the much better pressure recovery after the first pressure minimum that occurs with a fully turbulent boundary layer; the fully turbulent boundary layer can better resist the adverse pressure gradient before separating at $|\theta|=100$ deg on one side and $|\theta|=120$ deg on

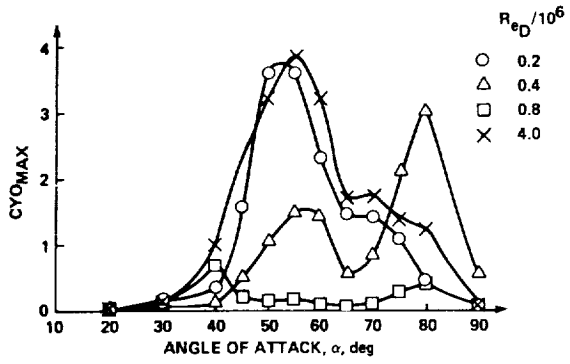

Fig. 7 Variation of maximum overall side force with angle of attack.

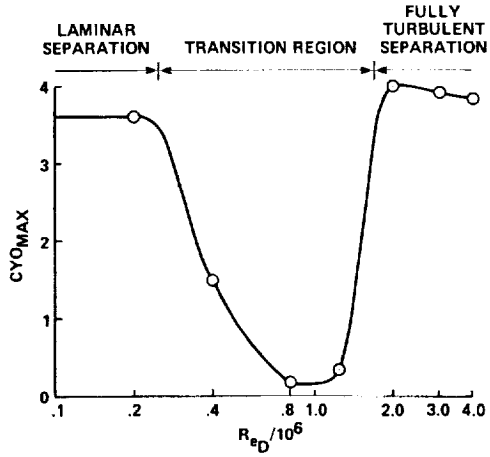

Fig. 8 Variation of maximum overall side force with Reynolds number at $\alpha=55$ deg.

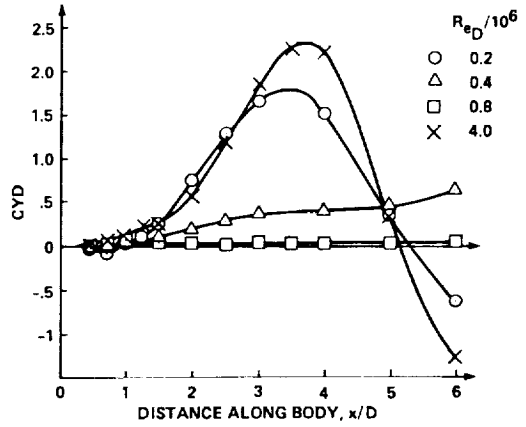

Fig. 9 Side force distributions at different Reynolds numbers.

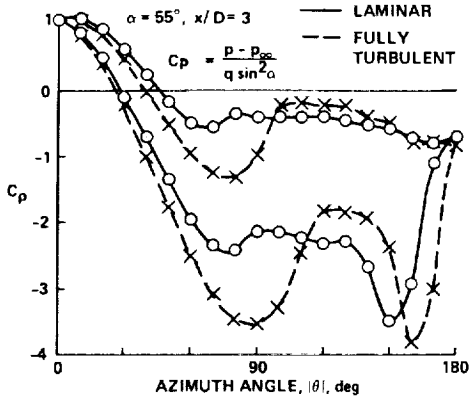

Fig. 10 Typical asymmetric pressure distributions for laminar and fully turbulent separation at $\alpha=55$ deg.

the other side. Note the distinct pressure minimums toward the rear of the model on the high suction side for both laminar and turbulent cases. These are caused by the rapid acceleration of the back flow from the rear attachment point before the flow separates and forms a secondary vortex rotating in the opposite direction with respect to the primary vortex on this side.

An example of an asymmetric pressure distribution at a station on the body experiencing transitional flow separation is presented in Fig. 11. This distribution occurred at $x/D=6$ in a test at an angle of attack of 55 deg and a Reynolds number of 0.4×10^6. It is radically different from the laminar and fully turbulent cases shown in Fig. 10. This latter figure showed that with laminar or fully turbulent separation, the asymmetry between the pressures on the two halves of the cylinder extended all the way from the windward to the leeward side of the cylinder. The transitional case (Fig. 11) shows that the asymmetry is confined to the flow in front of the separation lines at around $|\theta|$ of 120-130 deg. The time-averaged pressure behind these separation lines is nearly constant, and no distinct pressure minimums occur toward the rear of the cylinder for this transitional flow case. A variety of different forms of asymmetric pressure distributions can be found among the results with transitional separation; however, they all share the characteristics described previously. The asymmetric pressure distributions found here on an inclined cylinder are strikingly similar to the results obtained by Kamiya et al.[4] and Jones et al.[5] for two-dimensional cylinder flow in the transitional range of Reynolds number. Flow can vary from being near laminar on one side and transitional on the other, through different forms of transitional separation on each side (with and without laminar separation bubbles), to transitional on one side and fully turbulent on the other. None of these varieties of mixed flow on the inclined ogive cylinder produces local side-force coefficients (CYD) greater than 1.0. This agrees very well with the maximum value of $C_L=1.2$ quoted in Ref. 4 for two-dimensional cylinder flow in the transitional flow regime.

In summary, there would appear to be two different basic mechanisms for producing asymmetric flow and, hence, a side force on an ogive cylinder. One mechanism that occurs over a wide range of Reynolds number for both laminar and fully turbulent separation is where the side force results from asymmetric vortex patterns in the wake of the body, in the manner qualitatively represented by the impulsive flow analogy. The other mechanism, which occurs only in a narrow band of Reynolds numbers corresponding to the transitional separation regime, is where the side force results from asymmetry of the flow ahead of the primary separation lines, because different transitional states of the boundary layer occur on either side of the cylinder. The first mechanism is a much more powerful means of producing side force for the fineness ratio tested here ($L/D=6$) for angles of attack up to 70 deg. In addition, results in the laminar and fully turbulent separation regimes, where the first mechanism operates, were repeatable for a given α, Re_D, and ϕ setting, and maximum side force should be predictable for different fineness ratio bodies from the characteristic form of the side-force distribution. However, transitional separation cases, where the second mechanism operates, were often not repeatable and no characteristic form of side-force distribution can be determined. Indeed, the different transitional states of the boundary layer are probably triggered by minute details of the surface roughness on the model. No detailed side-force predictions seem likely in this transitional separation regime.

Normal Forces

It is now accepted that the side force on an ogive cylinder varies with roll orientation, but, in general, the current literature suggests that the normal force is affected only slightly. These results, obtained in a low-turbulence tunnel, where many high side-force cases occur, suggest that normal force can also be a strong function of roll orientation. This variation has already been demonstrated in Figs. 3 and 5. Hence, the variations of overall normal-force coefficient CNO with angle of attack, plotted in Fig. 12, are not single lines but bands of possible values. Note that the same Reynolds numbers have been chosen as examples as were used for overall side force in Fig. 7.

Once again, the laminar ($Re_D=0.2\times10^6$) and the fully turbulent ($Re_D=4.0\times10^6$) separation cases are of similar character. Both demonstrate wide bands of possible overall normal force in the angle-of-attack range (45-70 deg) where large side forces were recorded. As noted earlier (in the subsection on roll-angle effect), progressive increases in side force produce progressive increases in normal force. This increase in normal force for the highly asymmetric flow cases is produced in the high suction half of the cylinder by the second pressure minimum at the rear of the cylinder, which marks the rapid acceleration of the back flow from the rear attachment point. The wide variation of normal force for the results at a Reynolds number of 4.0×10^6 at angles of attack above 70 deg is not caused by differences between highly asymmetric and symmetric flow. Instead, it reflects the fact that for angles of attack above about 70 deg, a Reynolds number of 4.0×10^6 is close to the boundary between fully turbulent and transitional flow (see the following subsection), and both types of flow are represented among the results at different roll angles.

The transitional separation cases ($Re_D=0.4\times10^6$ and 0.8×10^6) show only small bands of variation with roll angle.

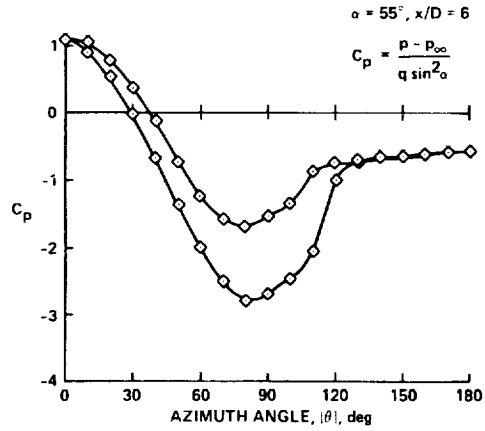

Fig. 11 Asymmetric pressure distribution in transitional flow regime.

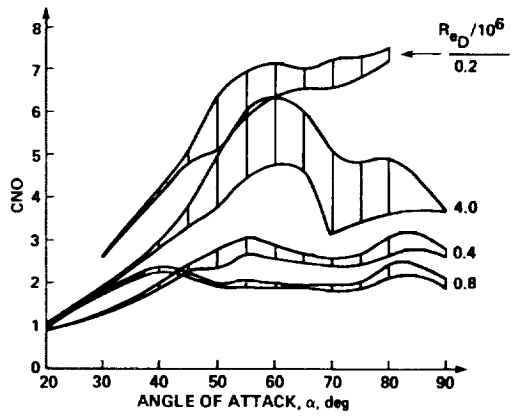

Fig. 12 Variation of normal force with angle of attack.

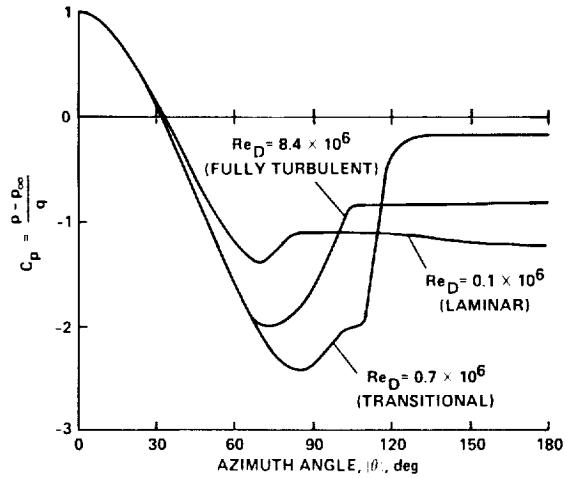

Fig. 13 Two-dimensional cylinder pressure distributions at different Reynolds numbers taken from Roshko.[6]

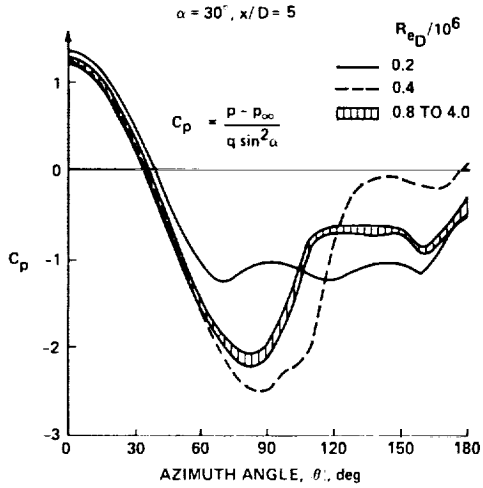

Fig. 14 Pressure distributions around inclined cylinder at different Reynolds numbers.

Note that at $\alpha = 80$ deg and $Re_D = 0.4 \times 10^6$, where some high and near-zero side-force results were obtained, the corresponding normal-force results varied only slightly. In contrast to the laminar and fully turbulent cases, higher side force was accompanied by lower normal force. This contrasting behavior of the normal-force results further emphasizes the existence of the two different flow mechanisms producing asymmetric flow, which were described in the subsection on side forces.

Critical Reynolds Numbers

For many years there has been a need to define critical Reynolds numbers to mark the boundaries between laminar, transitional, and fully turbulent separation conditions on inclined cylindrical bodies. Until these present results, there was a lack of direct information on how the critical Reynolds numbers varied with angle of attack. The better known critical Reynolds numbers at 90-deg incidence (two-dimensional cylinder flow) were extrapolated to cover the angle-of-attack range up to 90 deg. The first extrapolation that was tried derived from a strict application of cross flow theory. It based the Reynolds number on cross flow velocity and took the same critical value as for two-dimensional cylinder flow. This approach produces a critical Reynolds number based on freestream velocity and cylinder diameter

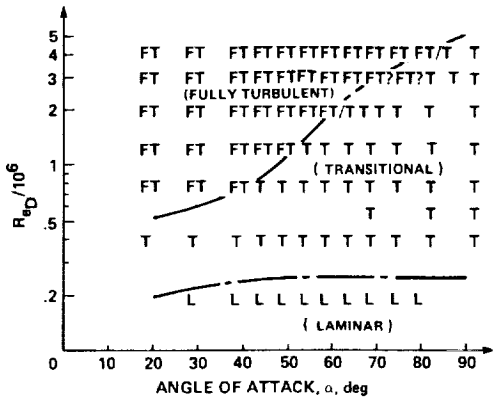

Fig. 15 Classification of results into three main flow regimes.

which increases as angle of attack is reduced from 90 deg toward zero. This variation with angle of attack does not seem reasonable and does not fit the available experimental evidence. Hence, Reynolds numbers based on characteristic lengths, which increased as angle of attack was reduced from 90 deg, came into favor. The most common of these uses a characteristic length equal to D cosec α. However, neither this characteristic length nor a number of variants on this theme has been successful enough in correlating all the available experimental data to be generally accepted.

The Reynolds number range covered in this testing was chosen with the hope that it would be sufficient to span laminar, transitional, and fully turbulent separation conditions for most of the angle-of-attack range from 20 to 90 deg. Classification of the flow, at a particular angle of attack and Reynolds number, into one of these three regimes was possible only because pressure distributions were monitored. Given a knowledge of typical pressure distributions in these three flow regimes for two-dimensional cylinder flow, it proved a simple matter to classify the flow on the inclined ogive cylinder. Figure 13 is reproduced from Roshko[6] to remind the reader of typical laminar, transitional, and fully turbulent pressure distributions from two-dimensional cylinder flow. Reference 7 is another useful source of information on flow around circular cylinders. As an example of this classification procedure, consider the pressure distributions at station $x/D = 5$ on the ogive cylinder, with the cylinder set at an angle of attack of 30 deg for a variety of Reynolds numbers. Pressure distributions for this case are presented in Fig. 14.

The solid line in Fig. 14 representing the results for a Reynolds number of 0.2×10^6 is typical of a laminar separation case with early boundary-layer separation around $|\theta| = 85$ deg. The results for a Reynolds number of 0.4×10^6 (dashed line) show evidence of a laminar separation bubble followed by turbulent reattachment, with final separation occurring at about $|\theta| = 140$ deg. At this angle of attack, all the results at Reynolds numbers of 0.8×10^6 and above had a common form (hatched band) that is very similar to the fully turbulent pressure distributions found in two-dimensional cylinder flow. The boundary layer is fully turbulent before its separation at around $|\theta| = 110$ deg. At higher angles of attack, a similar classification procedure could be used by choosing the most symmetrical flow cases, or the flow could be classified by distinguishing between the two types of asymmetric flow described in the subsection on side forces. The results at all test conditions were classified in this way. This classification was entered on a chart of Reynolds number against angle of attack. The letters L, T, and FT were used to denote laminar, transitional, and fully turbulent separation conditions, respectively. This chart is presented in Fig. 15.

The dashed lines are suggested boundaries between the three flow regimes. The construction of the boundary between

laminar and transitional separation was aided by the author's interpretation of Clark's results.[8] Note the totally different forms of the two boundaries between the three regimes. The critical Reynolds number boundary between transitional and fully turbulent separation is a strong function of angle of attack, whereas the laminar-transitional separation boundary varies much less with angle of attack. These critical Reynolds number boundaries should be applied only to smooth cylinders in low-turbulence streams. It seems likely that freestream turbulence and model surface roughness will have effects in inclined cylinder flow similar to those experienced in two-dimensional cylinder flow.[7] Increased surface roughness and increased freestream turbulence will probably lower the Reynolds number at which these boundaries occur.

Conclusions

1) These results show that it is essential to vary the roll angle of an axisymmetric ogive cylinder at high angles of attack in order to define fully all the possible flow conditions. Only then is it possible to interpret correctly the effects of changing angle of attack or Reynolds number.

2) Two basic mechanisms for producing asymmetric flow and, hence, side force are identifiable from these results. One mechanism, that of asymmetric vortex patterns in the model wake, operates in both the laminar and the fully turbulent separation regimes. The other, that of asymmetric flow on the model ahead of the primary separation lines, occurs only in the transitional separation regime. In general, the first mechanism is a more powerful means of producing side force.

3) Normal force as well as side force can vary with roll orientation. This variation of normal force is most marked in the fully turbulent separation regime.

4) The comprehensive nature of this test program and the choice of pressure instrumentation has made it possible to draw up critical Reynolds number boundaries between the laminar, transitional, and fully turbulent separation regimes throughout the angle-of-attack range from 20 to 90 deg for an ogive-cylinder configuration.

Acknowledgments

The author thanks everyone at Ames who contributed to the success of this project, particularly Gerald Malcolm, John Holmberg, and Richard Hanly.

References

[1] Lamont, P.J. and Hunt, B.L., "Pressure and Force Distributions on a Sharp-Nosed Circular Cylinder at Large Angles of Inclination to a Uniform, Subsonic Stream," *Journal of Fluid Mechanics*, Vol. 76, Pt. 3, 1976, pp. 519-559.

[2] Hunt, B.L. and Dexter, P.C., "Pressures on a Slender Body at High Angles of Attack in a Very Low Turbulence Level Air Stream," *AGARD Conference Proceedings No. 247, High Angle of Attack Aerodynamics*, Sandefjord, Norway, Paper 17, Oct. 1978.

[3] Dexter, P.C. and Hunt, B.L., "The Effects of Roll Angle on the Flow over a Slender Body of Revolution at High Angles of Attack," AIAA Paper 81-0358, 1981.

[4] Kamiya, S., Suzuki, S., and Nishi, T., "On the Aerodynamic Force Acting on a Circular Cylinder in the Critical Range of the Reynolds Number," AIAA Paper 79-1475, 1979.

[5] Jones, G.W., Cincotta, J.J., and Walker, R.W., "Aerodynamic Forces on a Stationary and Oscillating Circular Cylinder at High Reynolds Number," NASA TR R-300, Feb. 1969.

[6] Roshko, A., "Experiments on the Flow Past a Circular Cylinder at Very High Reynolds Number," *Journal of Fluid Mechanics*, Vol. 10, Pt. 3, 1961, pp. 345-356.

[7] "Fluid Forces Acting on Circular Cylinders for Application in General Engineering. Part 1. Long Cylinders in Two-Dimensional Flow," Engineering Sciences Data Item 70013, Engineering Sciences Data Unit, Oct. 1970.

[8] Clark, W.H., "Body Vortex Formation on Missiles in Incompressible Flows," AIAA Paper 77-1154, 1977.